Ocean Engineering 58 (2013) 208–216

Contents lists available at SciVerse ScienceDirect

Ocean Engineering

journal homepage: www.elsevier.com/locate/oceaneng

Unsteady RANS simulations of flow around rectangular cylinders with different aspect ratios

Xinliang Tian [a,*], Muk Chen Ong [b], Jianmin Yang [a], Dag Myrhaug [b]

[a] State Key Laboratory of Ocean Engineering, Shanghai Jiao Tong University, Shanghai 200240, China
[b] Department of Marine Technology, Norwegian University of Science and Technology, NO-7491 Trondheim, Norway

ARTICLE INFO

Article history:
Received 15 January 2012
Accepted 27 October 2012
Available online 12 December 2012

Keywords:
Numerical simulation
Rectangular cylinder
Aspect ratio
Plate

ABSTRACT

Flow around rectangular cylinders with different aspect ratios has been investigated using the two-dimensional (2D) Unsteady Reynolds-Averaged Navier–Stokes (URANS) equations with the k–ω Shear Stress Transport (SST) turbulence model. The aspect ratios ($R=B/H$, where B and H are the breadth and height of the cross-sections in the streamwise and cross-stream directions, respectively) of the cross-sections vary from 1 to 0.05. The Reynolds number (Re) based on the free stream velocity and H is 21,400. The objective of the present study is to evaluate the validity of 2D URANS simulations with k–ω SST model for the flow around rectangular cylinders. The drag forces acting on the cylinders with high aspect ratios (i.e. $R=1$, 0.8 and 0.6) are well predicted by the present simulations; however, the drag forces are overpredicted for low aspect ratios (i.e. $R=0.4$, 0.2, 0.1 and 0.05). The vortex shedding frequencies are not sensitive to the aspect ratio, and the values calculated in the present simulations are in good agreement with the published results. The effects of aspect ratios on the vortex formation have also been discussed.

1. Introduction

Flow around rectangular cylinders has been widely studied due to its importance in offshore engineering applications, e.g. columns of tension-leg platforms and pontoons of semi-submersibles. Unlike the case of the flow around circular cylinders, the flow separation point is fixed at the leading corners of the rectangular cross-section. The aspect ratio $R=B/H$, where B is the breadth along the direction of flow and H is the height of the cross-section, plays an important role in determining the vortex formation and the hydrodynamic forces on the body.

Several experimental studies on the effects of aspect ratios have been carried out. Nakaguchi et al. (1968) studied the aspect ratio effects for Reynolds number ($Re=U_\infty H/\nu$, where U_∞ is the free stream velocity and ν is the kinematic viscosity of the fluid) ranging from 2×10^4 to 6×10^4. A peak in the drag coefficient and a discontinuity in the Strouhal number ($St=fH/U_\infty$, where f is the vortex shedding frequency) near $R=0.6$ were demonstrated. Norberg (1993) also reported a similar conclusion from a wind tunnel experiment for rectangular cylinders with $R=1/3$–3 for Re from 400 to 3×10^4. Ohya (1994) investigated the base pressure variation of rectangular cylinders with $R=0.4$, 0.5 and 0.6 at $Re=6.7\times10^3-6.7\times10^4$, and pointed out that there was a sudden change in the flow pattern around the cylinder when $R=0.5$.

Several numerical studies on the effects of aspect ratios have also been carried out. Okajima (1990) investigated the two-dimensional (2D) laminar flow around rectangular cylinders with $R=0.6$–8 at $Re=150$–800 using a finite difference method. He reported that St and flow pattern change abruptly at the critical aspect ratios $R=2.8$ and 6. Aerodynamic characteristics of rectangular cylinders with $R=0.6$–8 were studied numerically by Shimada and Ishihara (2002) using a two-layer k–ε turbulence model. The results of the 2D simulations by Okajima (1990) and Shimada and Ishihara (2002) were in good agreement with experiments and three-dimensional (3D) calculations for $R=0.6$–8 (further details are given in their papers). Sohankar (2008) performed 3D large-eddy simulations (LES) for $R=0.4$–4 at $Re=10^5$.

Most of the 2D numerical investigations on the aspect ratio effect for flow around rectangular cylinders have been performed for $R\geq0.6$. To the authors' knowledge, the k–ω shear-stress transport (SST) model (Menter, 1994) has not been applied for the similar studies. The objective of the present study is to evaluate the validity of the 2D URANS simulations with the k–ω SST model for the flow around rectangular cylinders with different aspect ratios. The present study will focus on the low aspect ratios ($R\leq1$) and numerical simulations will be carried out for $R=$(1, 0.8, 0.6, 0.4, 0.2, 0.1 and 0.05) at $Re=21{,}400$. The hydrodynamic quantities, such as time-averaged pressure and drag

* Corresponding author. Tel.: +86 136 8195 7161; fax: +86 21 34207058
E-mail address: tianxinliang@sjtu.edu.cn (X. Tian).

0029-8018/$ - see front matter Crown Copyright © 2012 Published by Elsevier Ltd. All rights reserved.
http://dx.doi.org/10.1016/j.oceaneng.2012.10.013

coefficients, root-mean-square (r.m.s.) values of lift coefficients and Strouhal numbers are compared with the published experimental and numerical results. The effects of the aspect ratios on the vortex formation are also presented and discussed in details.

2. Mathematical formulation

2.1. Flow model

The Reynolds-averaged equations for conservation of mass and momentum are given by

$$\frac{\partial u_i}{\partial x_i}=0 \tag{1}$$

$$\frac{\partial u_i}{\partial t}+u_j\frac{\partial u_i}{\partial x_j}=-\frac{1}{\rho}\frac{\partial p}{\partial x_i}+\nu\frac{\partial^2 u_i}{\partial x_j\partial x_j}-\frac{\partial\overline{u_i'u_j'}}{\partial x_j} \tag{2}$$

where $i, j=1, 2$. Here x_1 and x_2 denote the streamwise and cross-stream directions, respectively; u_1 and u_2 are the corresponding mean velocity components; $\overline{u_i'u_j'}$ is the Reynolds stress component, where u_i' denotes the fluctuating part of the velocity; p is the pressure; ρ is the density of the fluid and t is the time.

The k–ω SST turbulence model (Menter, 1994) is used in the present study. The SST model combines the k–ω and the k–ε models, with the original k–ω model of Wilcox (1998) in the near-wall region and the standard k–ε model of Jones and Launder (1973) in the outer wake region and in the free shear layers. Following Menter et al. (2003), the equations for the SST model is taken as

$$\frac{D(\rho k)}{Dt}=\tilde{P}_k-\beta^*\rho\omega k+\frac{\partial}{\partial x_j}\left[(\mu+\sigma_k\mu_t)\frac{\partial k}{\partial x_j}\right] \tag{3}$$

$$\frac{D(\rho\omega)}{Dt}=\alpha\rho S^2-\beta\rho\omega^2+\frac{\partial}{\partial x_j}\left[(\mu+\sigma_\omega\mu_t)\frac{\partial\omega}{\partial x_j}\right]+2(1-F_1)\rho\sigma_{\omega2}\frac{1}{\omega}\frac{\partial k}{\partial x_j}\frac{\partial\omega}{\partial x_j} \tag{4}$$

where $\tilde{P}_k$ is given by

$$\tilde{P}_k=\min\left[\mu_t\frac{\partial u_i}{\partial x_j}\left(\frac{\partial u_i}{\partial x_j}+\frac{\partial u_j}{\partial x_i}\right),10\beta^*\rho k\omega\right] \tag{5}$$

If ϕ_1 represents any constant in the original k–ω model ($\sigma_{k1},\ldots$) and ϕ_2 represents any constant in the original k–ε model ($\sigma_{k2},\ldots$) , then ϕ, the corresponding constant of the new model given by Eqs. (3) and (4), is

$$\phi=F_1\phi_1+(1-F_1)\phi_2 \tag{6}$$

$$F_1=\tanh(\arg_1^4) \tag{7}$$

$$\arg_1=\min\left[\max\left(\frac{\sqrt{k}}{\beta^*\omega y},\frac{500\nu}{y^2\omega}\right),\frac{4\rho\sigma_{\omega2}k}{CD_{k\omega}y^2}\right] \tag{8}$$

$$CD_{k\omega}=\max\left(2\rho\sigma_{\omega2}\frac{1}{\omega}\frac{\partial k}{\partial x_j}\frac{\partial\omega}{\partial x_j},10^{-10}\right) \tag{9}$$

Here y is the distance to the nearest wall and $CD_{k\omega}$ is the positive portion of the cross-diffusion term of Eq. (4).

The turbulent eddy viscosity is defined as

$$\nu_t=\frac{a_1k}{\max(a_1\omega,SF_2)} \tag{10}$$

where S is the invariant measure of the strain rate and F_2 is given by

$$F_2=\tanh(\arg_2^2),\quad \arg_2=\max\left(2\frac{\sqrt{k}}{0.09\omega y},\frac{500\nu}{y^2\omega}\right) \tag{11}$$

The constants of SST are: $\beta^*=0.09$, $a_1=0.31$, $\alpha_1=0.5532$, $\alpha_2=0.4403$, $\beta_1=0.075$, $\beta_2=0.0828$, $\sigma_{k1}=0.85034$, $\sigma_{k2}=1.0$ and $\sigma_{\omega1}=0.5$, $\sigma_{\omega2}=0.85616$.

2.2. Numerical simulation scheme, computational domain and boundary conditions

The open source computational fluid dynamics (CFD) code *OpenFOAM* is used here. *OpenFOAM* is mainly applied for solving problems in continuum mechanics. It is developed based on the tensorial approach and object oriented techniques (Weller et al., 1998). The pressure implicit with splitting of operators (PISO) scheme (*pisoFoam*) is used in the present study. The spatial schemes for gradient, Laplacian and divergence are Gauss linear, Gauss linear corrected and Gauss linear schemes, respectively. All these schemes are in second order. The second order Crank–Nicolson scheme is used for the time integration. Further details of these schemes are given in OpenFOAM (2009).

The size of the whole computational domain is $35H$ by $20H$, and the origin of the coordinates is located at the center of the rectangular cylinder, see Fig. 1. The flow inlet boundary is located $10H$ upstream from the center of the cylinder and the flow outlet boundary is located $25H$ downstream from the center of the cylinder. The top and bottom boundaries are located at a distance of $10H$ from the center of the cylinder. These distances are large enough to eliminate the far field effects from the boundaries. The boundary conditions used for the simulations are set as follows:

(1) A uniform flow, $u_1=U_\infty$, $u_2=0$, is set at the inlet boundary; the pressure is specified as zero normal gradient at the inlet boundary. Moreover, k and ω at the inlet boundary are calculated as follows:

$$k_{inlet}=1.5(U_\infty I)^2 \tag{12}$$

where the turbulence intensity $I=2\%$ (Lyn et al., 1995)

$$\omega_{inlet}={k_{inlet}}^{0.5}/(C_\mu^{0.25}l) \tag{13}$$

where $C_\mu\approx0.09$ is the empirical constant specified in the turbulent model and turbulence length $l=0.07H$ (Rahman et al., 2007; Gao and Chow, 2005). Effects of l on the calculated results have been studied by using a much lower value ($l=0.04$ H) for the square cylinder, and small variations (less than 0.27%) are observed in the hydrodynamic quantities (i.e. mean drag coefficient, r.m.s. of lift coefficient and Strouhal number).

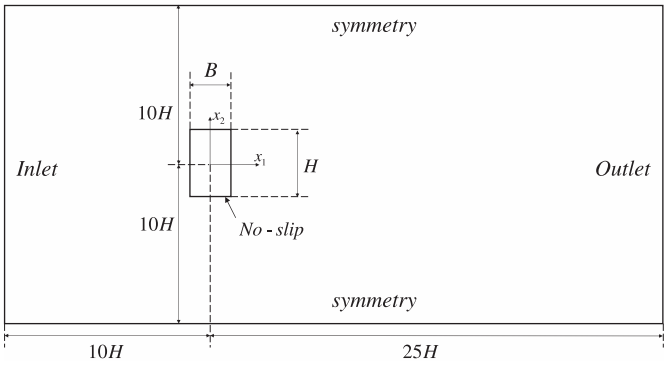

Fig. 1. Computational domain and boundary conditions.

(2) Along the outlet boundary, u_1, u_2, k and ω are specified as zero normal gradient; the pressure p is set as zero. The zero-pressure outlet boundary condition has been widely used to calculate the unsteady flow around bluff bodies (see e.g. Shimada and Ishihara, 2002; Sandham et al., 2003; Narasimhamurthy et al., 2010). Moreover, it has been checked carefully that the distance used in the present study from the outlet boundary to the body is far enough to eliminate the effects of the outlet boundary condition on the numerical results.

(3) On the surface of the cylinder, no-slip boundary condition is prescribed, i.e. $u_1 = u_2 = 0$; p is set as zero normal gradient; k is fixed at 0; ω is calculated as follows (Menter, 1994):

$$\omega_{body} = 10 \times \frac{6\nu}{\beta_1(\Delta y_1)^2} \tag{14}$$

where Δy_1 is the distance to the next point away from the cylinder surface, taken as $\Delta y_1 = 0.002$ H.

(4) Symmetric boundary conditions are applied for u_1, u_2, p, k and ω at the top and bottom boundaries.

2.3. Grid and time resolution tests

Both grid and time step tests have been carried out for all the cases with $R=1$, 0.8, 0.6, 0.4, 0.2, 0.1 and 0.05. The time-averaged drag coefficient ($\overline{C}_D$), the r.m.s. value of lift coefficient (C_{Lrms}) as well as St are considered in the tests. Here the drag coefficient (C_D) and lift coefficient (C_L) are defined as follows:

$$C_D = \frac{F_{x_1}}{\frac{1}{2}\rho U_\infty^2 H} \tag{15}$$

$$C_L = \frac{F_{x_2}}{\frac{1}{2}\rho U_\infty^2 B} \tag{16}$$

where F_{x_1} and F_{x_2} are the streamwise and cross-stream force components acting on the rectangular cylinder per unit length, respectively.

The hydrodynamic results of the cases with different grid and time resolutions are shown in Table 1, where Δt represents the time step and the relative change is calculated by taking the variation of hydrodynamic results between two consecutive meshes or time steps with respect to the median of them. For the square case ($R=1$), a grid convergence study has been carried out with four sets of meshes with 67,990–255,900 elements, see Table 1. The statistical quantities of hydrodynamic results are calculated from 10 vortex shedding cycles after the vortex shedding cycle has repeated itself. Moreover, the statistical uncertainty has been evaluated by comparing the hydrodynamic results of Case A3 obtained from 10 vortex shedding cycles with that obtained from 20 vortex shedding cycles. The difference of the results is always below 0.01%. Small variations are observed in the hydrodynamic quantities although the number of mesh elements increases about four times. The influence of the time step on the results is evaluated by comparing the results of the Cases A2 and A3; and small variations of the hydrodynamic results are observed. For the other aspect ratios, similar grid and time step tests are carried out with three cases for each aspect ratio in which the first and second cases are carried out for grid resolution test and the second and third cases are carried out for time resolution test. The variations of the hydrodynamic results of two consecutive cases are less than 3%. It should be noted that smaller time steps are used for $R=0.6$ than for the other aspect ratios in order to achieve a small variation of the hydrodynamic results. An example of the mesh structures for $R=0.4$ with 64,144 elements is presented in Fig. 2.

A near-wall grid refinement test is also carried out for the square case ($R=1$). The results of $\overline{C}_D$, C_{Lrms} and St do not change significantly as the distance of the first node away from the cylinder surface (Δy_1) varies in the range of [0.0015 H,0.004 H], see Table 2. In the present study, Δy_1 is fixed at 0.002 H. For the Case A3 ($R=1$) in Table 2, the values of y^+ over the entire wall boundaries range from 0 to 8.4 with an averaged value of 2.4, where $y^+ = u_*\Delta y_1/\nu = \sqrt{\tau_w/\rho}\Delta y_1/\nu$, where u_* and τ_w denote the wall friction velocity and wall shear stress, respectively. Similar procedure is taken to calculate the averaged y^+ for the other aspect ratios, and the averaged values of y^+ for seven considered aspect ratios give a range of 2.4–3.7.

Overall, it is concluded that the present simulations can provide satisfactory spatial and time resolutions for all the seven aspect ratios at $Re=21{,}400$. All the results presented in the

Table 1
Results of the cases with different grid and time resolutions.

R	Case	Elements	$\Delta t U_\infty/H$	$\overline{C}_D$	Relative change (%)	C_{Lrms}	Relative change (%)	St	Relative change (%)
1	A1	67,990	0.006	2.048	–	1.461	–	0.138	–
	A2	77,670	0.006	2.054	0.29	1.491	2.03	0.137	0.73
	A3[a]	77,670	0.004	2.060	0.29	1.492	0.07	0.138	0.73
	A4	145,020	0.004	2.059	0.05	1.493	0.07	0.136	1.46
	A5	255,900	0.004	2.060	0.05	1.493	0.00	0.136	0.00
0.8	B1	57,996	0.006	2.555	–	2.151	–	0.148	–
	B2	67,176	0.006	2.564	0.35	2.167	0.74	0.148	0.00
	B3[a]	67,176	0.004	2.575	0.43	2.162	0.23	0.149	0.67
0.6	C1	45,800	0.002	2.880	–	2.359	–	0.163	–
	C2	55,790	0.002	2.883	0.10	2.374	0.63	0.162	0.62
	C3[a]	55,790	0.001	2.866	0.59	2.348	1.10	0.162	0.00
0.4	D1	57,256	0.006	3.412	–	3.009	–	0.127	–
	D2	64,144	0.006	3.398	0.41	3.005	0.13	0.129	1.56
	D3[a]	64,144	0.004	3.371	0.80	3.065	1.98	0.131	1.54
0.2	E1	52,016	0.006	3.720	–	3.473	–	0.123	–
	E2	61,568	0.006	3.730	0.27	3.486	0.37	0.124	0.81
	E3[a]	61,568	0.004	3.699	0.83	3.393	2.70	0.126	1.60
0.1	F1	52,944	0.006	3.559	–	3.408	–	0.123	–
	F2	62,064	0.006	3.556	0.08	3.399	0.26	0.123	0.00
	F3[a]	62,064	0.004	3.531	0.71	3.335	1.90	0.126	2.41
0.05	G1	72,848	0.006	3.480	–	3.500	–	0.124	–
	G2	82,406	0.006	3.478	0.06	3.490	0.29	0.124	0.00
	G3[a]	82,406	0.004	3.446	0.92	3.390	2.91	0.127	2.39

[a] The final case for analyses.

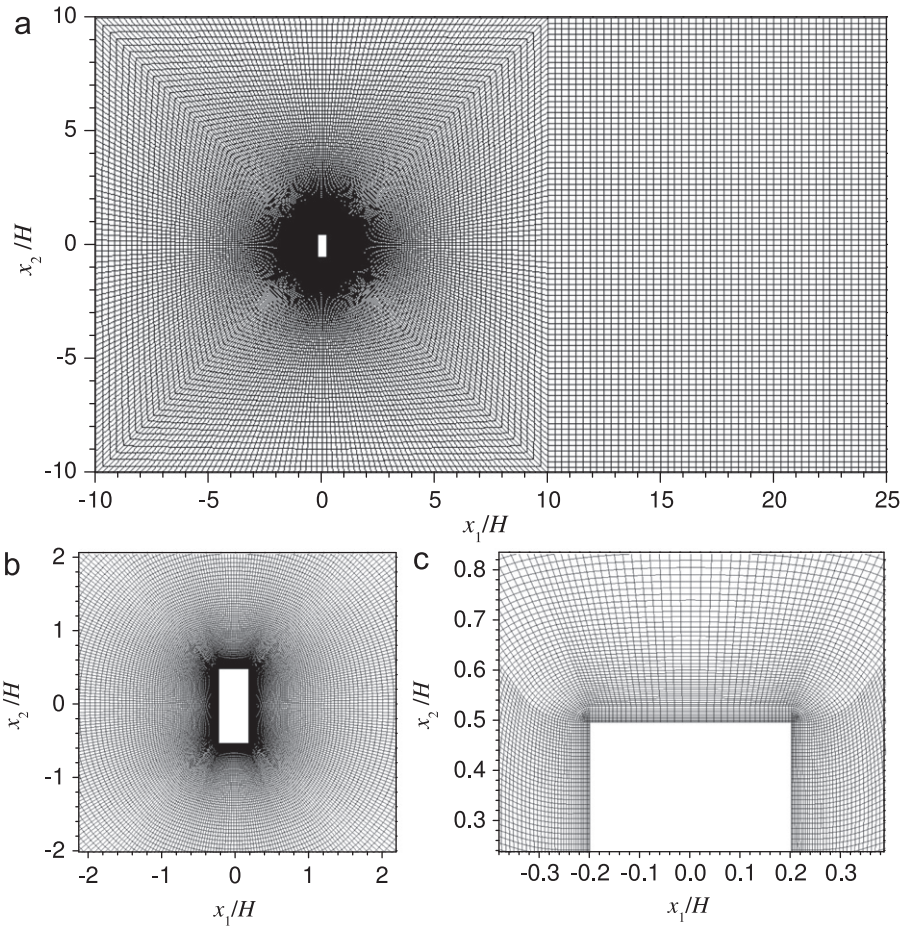

Fig. 2. An example of the mesh ($R=0.4$) with 64,144 elements: (a) whole computational domain, (b) grids around the cylinder and (c) grids around the corners.

Table 2
Results of the near-wall grid refinement test for $R=1$.

R	Case	Elements	$\Delta t U_\infty/H$	$\Delta y_1/H$	$\overline{C}_D$	C_{Lrms}	St
1	A6	77,670	0.004	0.0015	2.059	1.496	0.138
1	A3	77,670	0.004	0.002	2.060	1.492	0.138
1	A7	77,670	0.004	0.003	2.066	1.479	0.139
1	A8	77,670	0.004	0.004	2.066	1.464	0.139

following sections are obtained from the case labeled by "a" in Table 1.

3. Results and discussion

3.1. Square cylinder

First, the performance of the 2D URANS simulation with the k–ω SST turbulence model for the flow around a square cylinder ($R=1$) at $Re=21{,}400$ is discussed. Table 3 shows the hydrodynamic quantities, such as $\overline{C}_D$, C_{Lrms} and St obtained from the present simulations and published experiments (Lyn et al., 1995; Durao et al., 1988) as well as published numerical studies (Murakami and Mochida, 1995; Farhadi and Rahnama, 2005; Arslan et al., 2010; Bosch and Rodi, 1998; Shimada and Ishihara, 2002). The present predicted $\overline{C}_D$ is in good agreement with both the published experimental and numerical results. The reported numerical results of C_{Lrms} show a large variation of the values. This may be due to the different settings in these numerical studies, e.g. spanwise extension of the cylinder, blockage ratio and turbulence model. The present predicted C_{Lrms} is within the range of the published numerical results. The present predicted St is also in good agreement with both the published experimental and numerical results.

The distributions of the time-averaged pressure coefficient ($\overline{C}_p$) on the surfaces of the square ($R=1$) section are plotted in Fig. 3. The pressure coefficient is defined as

$$C_p = \frac{p-p_\infty}{\frac{1}{2}\rho U_\infty^2} \tag{17}$$

where the reference pressure p_∞ is taken as the pressure at the center of the inlet boundary. As shown in Fig. 3, on the front side of the square ($0 \le x_p \le 0.5$), the distribution of $\overline{C}_p$ calculated in the present study is in good agreement with the published experimental data (Otsuki et al., 1978; Bearman and Obasaju, 1982; Lee, 1975) and numerical results (Shimada and Ishihara, 2002). On the side-surface ($0.5 \le x_p \le 1.5$) and the back surface ($1.5 \le x_p \le 2$), $\overline{C}_p$ distributions do not show a large variation and the present calculated $\overline{C}_p$ agrees well with the experimental data (Otsuki et al., 1978; Bearman and Obasaju, 1982; Lee, 1975) and numerical results (Tamura and Ito, 1996; Shimada and Ishihara, 2002). Overall, the pressure distributions on the surfaces of square ($R=1$) are well predicted in the present study.

The mean streamwise velocity distribution along the center-line ($x_2=0$) of the square is shown in Fig. 4. In front of the cylinder, the numerical results agree well with each other and with the experimental results by Durao et al. (1988) except for $x_1/H<-1.5$. In the wake region, the present results agree reasonably well with the results of Shimada and Ishihara (2002) using a modified k–ε turbulence model. Both simulations underestimate the measured

Table 3
Hydrodynamic quantities for square cylinder ($R=1$).

No.	Author	Method	*Re*	$\overline{C}_D$	C_{Lrms}	*St*
1	Present	k–ω SST	21,400	2.060	1.492	0.138
2	Lyn et al. (1995)	Exp.	21,400	2.1	–	0.132
3	Durao et al. (1988)	Exp.	14,000	–	–	0.1382
4	Murakami and Mochida (1995)	LES (3D)	22,000	2.09	1.6	0.132
5	Farhadi and Rahnama (2005)	LES (3D)	21,400	2.306	0.984	0.138
6	Arslan et al. (2010)	LES (3D)	22,000	2.11	1.16	0.132
7	Bosch and Rodi (1998)	k–ε (2D)	22,000	2.108	1.012	0.146
8	Shimada and Ishihara (2002)	k–ε (2D)	22,000	2.05	1.43	0.141

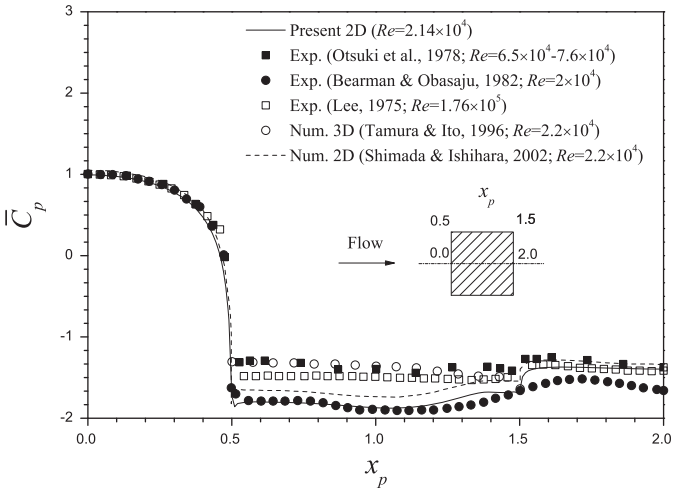

Fig. 3. Time-averaged pressure distributions on the surfaces of the square section ($R=1$).

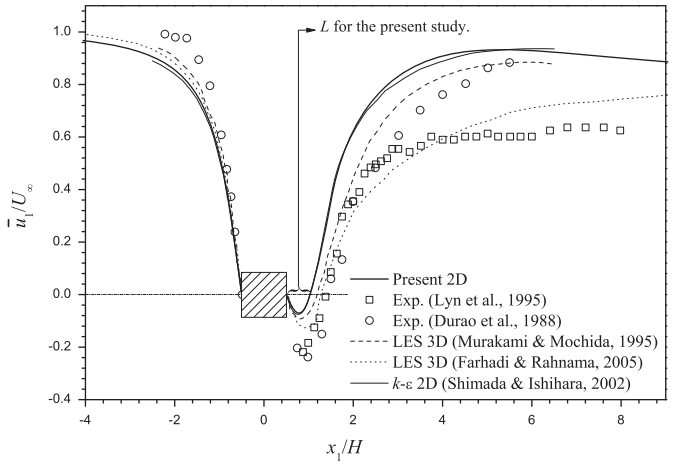

Fig. 4. Mean streamwise velocity distribution along the center-line of the square.

length of the mean recirculation region (L). The 3D LES results reported by Murakami and Mochida (1995) and Farhadi and Rahnama (2005) show a better agreement with the experimental results than the 2D URANS simulations; however, the LES results still underestimated the measured recirculation length. Moreover, the 2D URANS simulations reported by both the present study and Shimada and Ishihara (2002) give a more underestimation of the negative centreline velocity than the 3D LES results by Murakami and Mochida (1995) and Farhadi and Rahnama (2005), as compared with the experimental data by Lyn et al. (1995) and Durao et al. (1988).

Overall, the present k–ω SST model appears to give satisfactory hydrodynamic results for the square case ($R=1$) based on

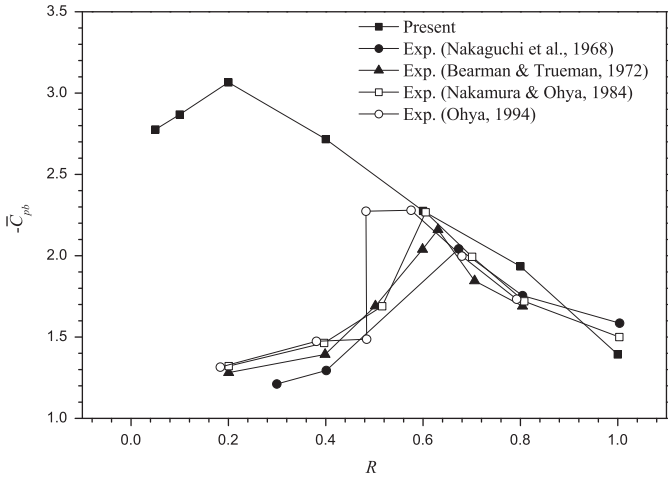

Fig. 5. Variation of mean base pressure coefficient ($\overline{C}_{pb}$) with aspect ratio (R).

the comparison with the published experimental and numerical results, although both the recirculation length and the negative centreline velocity (in absolute value) are underestimated.

3.2. Effect of R on hydrodynamic characteristics

The hydrodynamic quantities, such as mean base pressure coefficient ($\overline{C}_{pb}$), $\overline{C}_D$, C_{Lrms} and *St* are presented and compared with the published numerical and experimental results in this section. The $\overline{C}_{pb}$ refers to the averaged $\overline{C}_p$ over the back side of the cylinder.

Fig. 5 shows $-\overline{C}_{pb}$ versus R. It appears that $-\overline{C}_{pb}$ is in reasonably good agreement with the experimental results (Nakaguchi et al., 1968; Bearman and Trueman, 1972; Nakamura and Ohya, 1984; Ohya, 1994) for $R=1$, 0.8 and 0.6. However, the present 2D simulations are not able to predict the decreasing trend of $-\overline{C}_{pb}$ as R decreases for $R<0.6$. According to the open literature, the maximum $-\overline{C}_{pb}$ should be encountered at $R\approx 0.6$ (Nakaguchi et al., 1968; Bearman and Trueman, 1972; Nakamura and Ohya, 1984). The present simulations show that the maximum $-\overline{C}_{pb}$ is approximately at $R=0.2$; $-\overline{C}_{pb}$ is overpredicted for $R<0.6$.

Fig. 6 shows $\overline{C}_D$ versus R. The trend of $\overline{C}_D$ is very similar with $-\overline{C}_{pb}$, as shown in Fig. 5. The present results for $R=1$, 0.8 and 0.6 agree well with the results of Norberg (1993), Lyn et al. (1995) and Sohankar (2008). Bruno et al. (2010) performed a 3D LES for flows around a long rectangular cylinder ($R=5$) by using the orthogonal decomposition technique to analyze the fluctuating pressure field. They commented that the main phenomena which drive the forces on the rectangular cylinder remain 2D, although the 3D flow features are not negligible. However, the present predicted $\overline{C}_D$ is much higher than the experimental results (Norberg, 1993; Fage and Johansen, 1927) and 3D numerical results (Sohankar, 2008; Narasimhamurthy and Andersson, 2009; Najjar and Vanka, 1995a) for the lower aspect ratios (i.e. $R<0.6$).

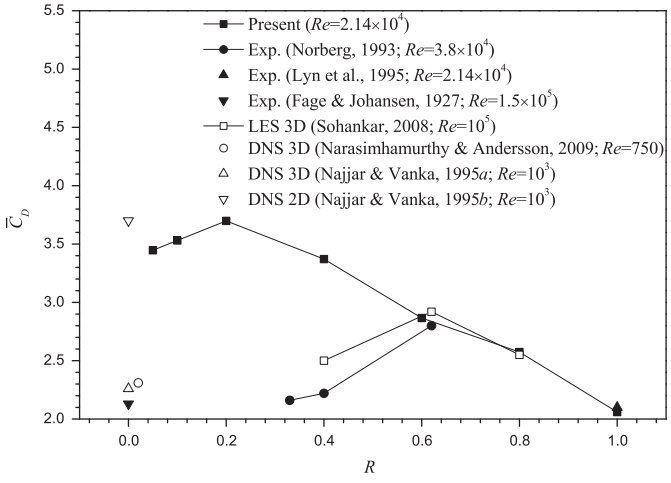

Fig. 6. Variation of mean drag coefficient ($\overline{C}_D$) with aspect ratio (R) (Najjar and Vanka, 1995b).

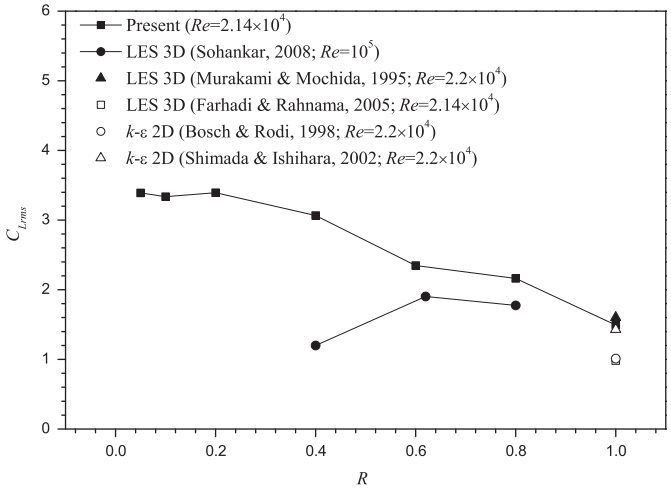

Fig. 7. Variation of r.m.s. lift coefficient (C_{Lrms}) with aspect ratio (R) (Najjar and Vanka, 1995b).

Najjar and Vanka (1995a) compared the 2D and 3D direct numerical simulation (DNS) results of a flat plate ($R=0$) at a lower Reynolds number (i.e. $Re=10^3$), and reported large discrepancies between their 2D and 3D results. Najjar and Vanka (1995a) further commented that 3D effects should be included in the simulation for the flow around a normal flat plate. Lisoski (1993) also found large differences between his 2D discrete vortex simulations and his experiments at $Re=1\times10^3$–1.25×10^4.

Fig. 7 shows C_{Lrms} versus R. It appears that the present predicted C_{Lrms} results have a qualitatively similar trend with that of the 3D LES studies (Sohankar, 2008) for $R\geq0.6$. For $R<0.6$, the present predicted C_{Lrms} shows an increasing trend as R decreases, which is contrary to the trend obtained by Sohankar (2008). This again shows that the 2D URANS simulations with the k–ω SST model does not give accurate predictions for $R<0.6$.

Fig. 8 shows St versus R. It appears that there is a reasonably good agreement between the present predicted St results and the published experimental data (Knisely, 1990; Fage and Johansen, 1927; Norberg, 1993; Lyn et al., 1995) as well as the published numerical results (Sohankar, 2008). It is apparent from the existing data that St is insensitive to the aspect ratio and all these results for different aspect ratios obtained by different authors are within the range of 0.144 ± 0.018. Moreover, the present predicted St values for $R=1$, 0.8 and 0.6 are slightly higher than both

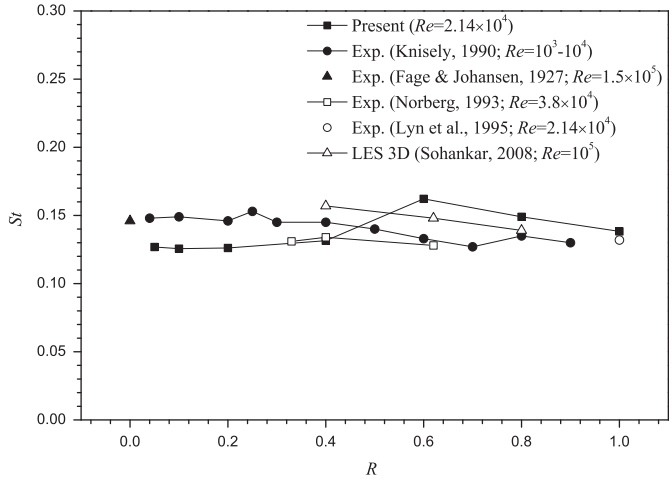

Fig. 8. Variation of Strouhal number (St) with aspect ratio (R).

the published experimental and numerical results, while the St values for $R=0.4$, 0.2, 0.1 and 0.05 are slightly lower than the published experimental data. The increasing trend of St between $R=0.4$ and $R=0.6$ is contrary to the decreasing trend in the experimental (Knisely, 1990; Norberg, 1993) and 3D LES (Sohankar, 2008) investigations. Therefore, the present k–ω SST model is not able to give an accurate prediction of the trend of St with respect to the aspect ratio.

Generally, the present 2D URANS simulations with k–ω SST model are able to give good predictions of the hydrodynamic results for $R\geq0.6$. However, for $R<0.6$, $-\overline{C}_{pb}$ and $\overline{C}_D$ are over-predicted by the present simulations as compared with the published experimental and 3D LES and DNS numerical results. This might be due to that the 3D effects which are more important for the low aspect ratio cases could not be predicted accurately by the present 2D URANS with the k–ω SST turbulence model. Shur et al. (2005) carried out 3D detached-eddy simulations (DES), 2D and 3D URANS simulations with three different turbulence models (i.e. Spalart and Allmaras (S–A), S–A with the rotation-curvature correction (SARC), and the two-equation shear–stress transport model of Menter (M-SST)) for three different nominally 2D bluff bodies flows (i.e. an airfoil at 90° attack angle, a circular cylinder and a rounded square cylinder). The URANS approach was exercised at a range of spanwise periods to explore its ability to select and sustain 3D flow structures, in a manner similar to DNS/LES/DES. They found that the 3D character indeed is present in all cases. Even though the 3D URANS is generally more accurate than the 2D URANS, it is less accurate than DES/LES. Shur et al. (2005) further commented that the flow structures in URANS are more energetic and smoother, and the small eddies are suppressed. Moreover, the method is rather unpredictable because it is sensitive to the initial field, turbulence model and spanwise size. Mannini et al. (2010) also commented briefly about this feature in their study on flow around a 5:1 rectangular cylinder. Shur et al. (2005) mentioned that 3D URANS simulations must be conducted using a significantly larger spanwise size than those necessary to develop three-dimensionality in DES/LES. Based on the numerical results reported by Shur et al. (2005), the 3D URANS gives worse comparison with the experimental data for the case of flow around an airfoil at 90° attack angle than for the cases of flows around a circular cylinder and a rounded square cylinder. It appears that the shape of the bluff body will also influence the numerical results of the 3D URANS. On the other hand, 3D LES (Tian et al., 2012; Sohankar, 2008) and 3D DNS (Najjar and Vanka, 1995a; Narasimhamurthy

and Andersson, 2009) have shown good numerical prediction for the flow around a thin plate. Thus, 3D LES/DES/DNS simulations, which are known to capture 3D flow structures well, are recommended for the low aspect ratio cases ($R<0.6$).

3.3. Effect of R on vortex formation

It is of interest to discuss the effects of R on the vortex formation around the rectangular cylinders, even though the drag coefficients have been found to be overpredicted for low aspect ratios, i.e. $R=0.4$, 0.2, 0.1 and 0.05. Fig. 9 shows the vorticity ($\Omega=\partial u_2/\partial x_1-\partial u_1/\partial x_2$) contours around the cylinders for $R=$ (1,0.8,0.6,0.4,0.2,0.1,0.05) when the lift force is maximum. The mode of vortex formation affects the pressure around the cylinders, and subsequently changes the drag force acting on the cylinders. The effects of R on the vortex formation are summarized as follows:

(1) The flow separates at the leading corners of the rectangular cylinders and the formed shear layer moves downstream with the main flow. For the cylinders with large aspect ratios (i.e. a long top or bottom side), the shear layer interacts with the side edges and the rear corners before it reaches the back side of the

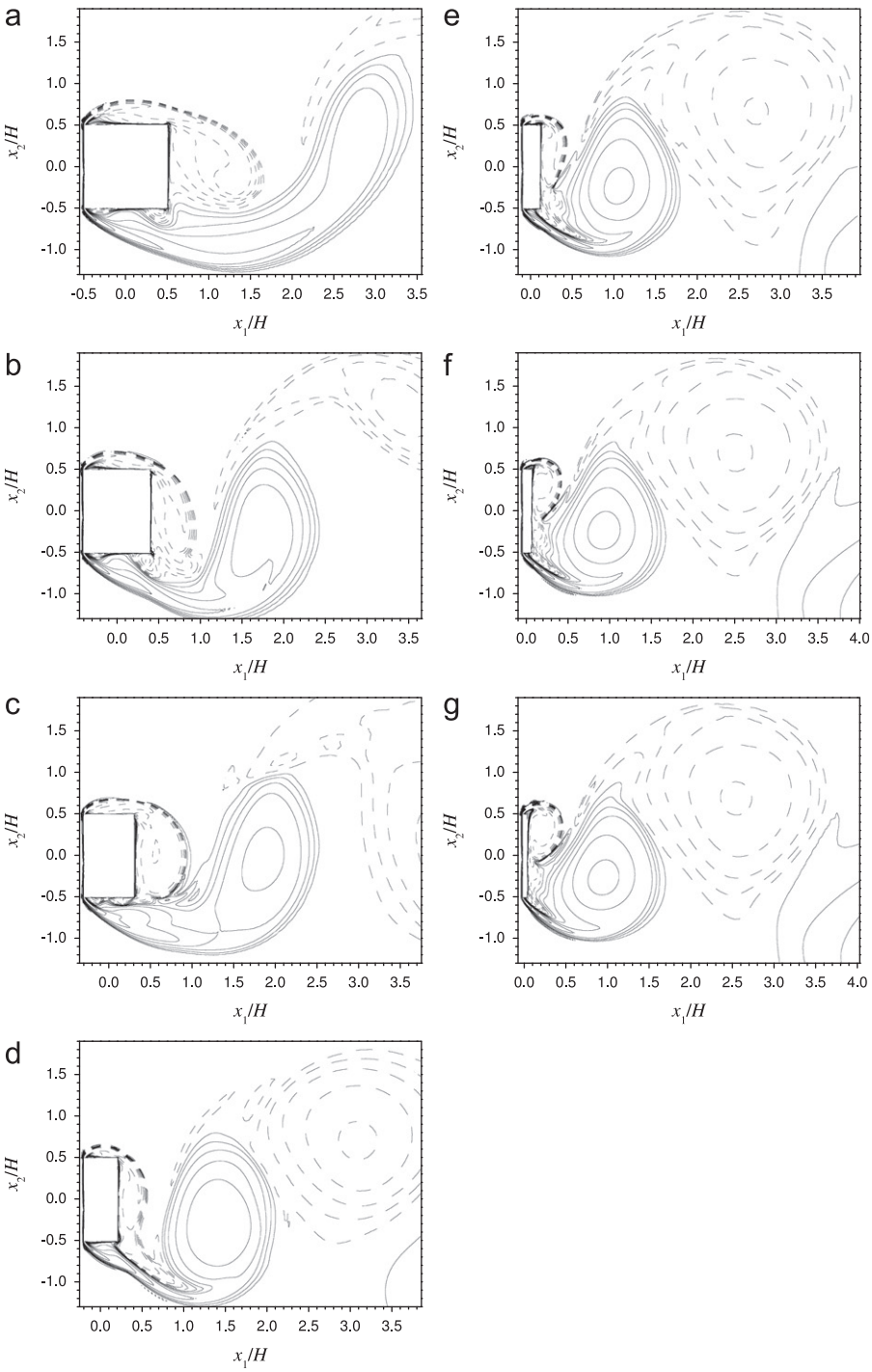

Fig. 9. Instantaneous vorticity contours in the near wake when the lift force is maximum. 16 levels of Ω from $-32U_\infty/H$ to $32U_\infty/H$ are plotted. The solid contour lines indicate the positive vorticity contours (counter-clockwise) and the dashed lines indicate the negative vorticity contours (clockwise).

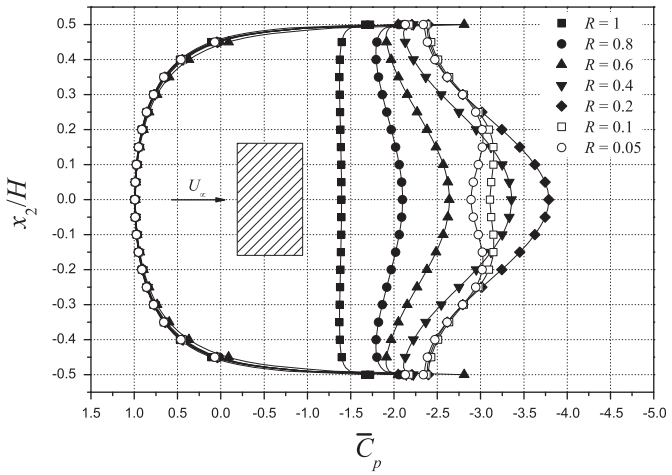

Fig. 10. The mean pressure coefficient ($\overline{C}_p$) along front and back sides of the cylinders with different aspect ratios.

cylinders. Bearman and Trueman (1972) also suggested that for cylinders with large aspect ratios the vortices are forced to form further downstream due to the influence of the rear corners. Thus, the high base pressure ($\overline{C}_{pb}$) and low drag ($\overline{C}_D$) occur in the large aspect ratio cases, see Figs. 5 and 6.

(2) As R decreases below 0.2, the length of the back side covered by the vortex decreases, see Fig. 9(e–g). In this case, the vortex becomes weaker near the back side of the rectangular cylinder as R decreases, and consequently the drag force decreases, see Fig. 6.

These two modes of vortex formation suggest a possible explanation of the drag force variation versus R. Generally, the first effect takes places for large aspect ratio cases ($R \gtrapprox 0.2$) while the second effect dominates for low aspect ratio cases ($R \lesssim 0.2$).

Furthermore, Fig. 10 shows the distributions of the mean pressure coefficient ($\overline{C}_p$) along the front and back sides of the cylinders with different aspect ratios. As shown, the pressure distribution on the front side for all the considered aspect ratios collapse together; thus, the differences in drag are mainly due to the differences in the pressure distributions along the back side. For the cases with $R \gtrapprox 0.2$, a reduction in the pressure as R decreases is found along the entire back side of the cylinder. However, for the cases with $R \lesssim 0.2$, the pressure in the region $|x_2|/H < 0.25$ increases as R decreases, while the pressure in the region $|x_2|/H > 0.25$ is only slightly influenced as R decreases. Therefore, it appears that the reduction of $\overline{C}_D$ for $R \leq 0.2$ is due to the increase of the pressure in the center part ($|x_2|/H < 0.25$) on the back side of the cylinder.

4. Conclusions

The flow normal to rectangular cylinders with different aspect ratios, i.e. $R=1$, 0.8, 0.6, 0.4, 0.2, 0.1 and 0.05, has been calculated numerically using the k–ω SST turbulence model at $Re=21{,}400$. The objective of this study has been to identify clearly the validity of 2D URANS simulations. The hydrodynamic characteristics have been calculated and compared carefully with the published experimental and numerical results. The vortex shedding mechanisms have also been studied. The main conclusions are summarized as follows:

(1) For the rectangular cylinders with $R=1$, 0.8 and 0.6, the present predicted $\overline{C}_D$ is in good agreement with the published experimental data and numerical results. However, the present 2D simulations with k–ω SST turbulence model are not able to give satisfactory results of $\overline{C}_D$ compared with the published experimental data for $R=0.4$, 0.2, 0.1 and 0.05.

(2) The present predicted C_{Lrms} for $R=1$ is within the range of the published numerical results. The present study provides a qualitatively similar trend of C_{Lrms} with respect to R as the 3D LES results at $Re=10^5$ by Sohankar (2008) for $R \geq 0.6$. However, for $R < 0.6$, the trend of C_{Lrms} with respect to R predicted in the present study is contrary to the 3D LES results by Sohankar (2008).

(3) The values of St is not sensitive to the aspect ratio, and the calculated St in this study agree well with the published experimental and numerical results, although the trend of St with respect to R is not accurately predicted.

(4) The increasing–decreasing trend of $\overline{C}_D$ versus R is explained by two different modes of vortex formation. The present prediction of the critical aspect ratio, at which a maximum drag force occurs, is at $R=0.2$ and that is much smaller than value of $R=0.6$ obtained from the experimental results.

Overall, it appears that the present 2D URANS simulations with k–ω SST model give satisfactory hydrodynamic results compared with the published experimental and numerical results for $R \geq 0.6$. For $R < 0.6$, 3D LES/DES/DNS which are known to capture 3D flow features well are recommended.

Acknowledgment

This work has been supported by National Natural Science Foundation of China (Grant no. 50979057) and China Scholarship Council (CSC). This support is gratefully acknowledged. The authors would also like to thank the editor and anonymous referees for their comments which have led to a much improved paper.

References

Arslan, T., Andersson, H.I., Pettersen, B., 2010. Calculation of vortex shedding around the bluff bodies by using LES model. In: ICCFD-6 of the Sixth International Conference on Computational Fluid Dynamics, St. Petersburg, Russia, pp. 293–294.

Bearman, P.W., Obasaju, E.D., 1982. An experimental study of pressure fluctuations on fixed and oscillating square-section cylinders. J. Fluid Mech. 119, 297–321.

Bearman, P.W., Trueman, D.M., 1972. An investigation of the flow around rectangular cylinders. Aero. Q. 23, 229–237.

Bosch, G., Rodi, W., 1998. Simulation of vortex shedding past a square cylinder with different turbulence models. Int. J. Numer. Methods Fluids 28, 601–616.

Bruno, L., Fransos, D., Coste, N., Bosco, A., 2010. 3D flow around a rectangular cylinder: a computational study. J. Wind Eng. Ind. Aerodyn. 98, 263–276.

Durao, D.F.G., Heitor, M.V., Pereira, J.C.F., 1988. Measurements of turbulent and periodic flows around a square cross-section cylinder. Exp. Fluids 6, 298–304.

Fage, A., Johansen, F.C., 1927. On the flow of air behind an inclined flat plate of infinite span. Proceedings of the Royal Society of London Series A, Containing Papers of a Mathematical and Physical Character 116, 170–197.

Farhadi, M., Rahnama, M., 2005. Three-dimensional study of separated flow over a square cylinder by large eddy simulation. Proceedings of the Institution of Mechanical Engineers Part G: J. Aero. Eng. 219, 225–234.

Gao, Y., Chow, W.K., 2005. Numerical studies on air flow around a cube. J. Wind Eng. Ind. Aerodyn. 93, 115–135.

Jones, W.P., Launder, B.E., 1973. The calculation of low-Reynolds-number phenomena with a two-equation model of turbulence. Int. J. Heat Mass Transfer 16, 1119–1130.

Knisely, C.W., 1990. Strouhal numbers of rectangular cylinders at incidence: a review and new data. J. Fluids Struct. 4, 371–393.

Lee, B.E., 1975. The effect of turbulence on the surface pressure field of a square prism. J. Fluid Mech. 69, 263–282.

Lisoski, D., 1993. Nominally 2-dimensional flow about a normal flat plate. Ph.D. Thesis, California Institute of Technology.

Lyn, D.A., Einav, S., Rodi, W., Park, J.H., 1995. A laser-Doppler velocimetry study of ensemble-averaged characteristics of the turbulent near wake of a square cylinder. J. Fluid Mech. 304, 285–319.

Mannini, C., Soda, A., Schewe, G., 2010. Unsteady RANS modelling of flow past a rectangular cylinder: investigation of Reynolds number effects. Comput. Fluids 39, 1609–1624.

Menter, F.R., 1994. Two-equation eddy-viscosity turbulence models for engineering applications. AIAA J. 32, 1598–1605.

Menter, F.R., Kuntz, M., Langtry, R., 2003. Ten years of industrial experience with the SST turbulence model. Turbul. Heat Mass Transfer 4, 625–632.
Murakami, S., Mochida, A., 1995. On turbulent vortex shedding flow past 2D square cylinder predicted by CFD. J. Wind Eng. Ind. Aerodyn. 54, 191–211.
Najjar, F.M., Vanka, S.P., 1995a. Effects of intrinsic three-dimensionality on the drag characteristics of a normal flat plate. Phys. Fluids 7, 2516–2518.
Najjar, F.M., Vanka, S.P., 1995b. Simulations of the unsteady separated flow past a normal flat plate. Int. J. Numer. Methods Fluids 21, 525–547.
Nakaguchi, H., Hashimoto, K., Muto, S., 1968. An experimental study on aerodynamic drag of rectangular cylinders. J. Jpn. Soc. Aero. Space Sci. 16, 5.
Nakamura, Y., Ohya, Y., 1984. The effects of turbulence on the mean flow past two-dimensional rectangular cylinders. J. Fluid Mech. 149, 255–273.
Narasimhamurthy, V.D., Andersson, H.I., 2009. Numerical simulation of the turbulent wake behind a normal flat plate. Int. J. Heat Fluid Flow 30, 1037–1043.
Narasimhamurthy, V.D., Andersson, H.I., Pettersen, B.R., 2010. Cellular vortex shedding in the wake of a tapered plate. J. Fluid Mech. 617, 355–379.
Norberg, C., 1993. Flow around rectangular cylinders: pressure forces and wake frequencies. J. Wind Eng. Ind. Aerodyn. 49, 187–196.
Ohya, Y., 1994. Note on a discontinuous change in wake pattern for a rectangular cylinder. J. Fluids Struct. 8, 325–330.
Okajima, A., 1990. Numerical simulation of flow around rectangular cylinders. J. Wind Eng. Ind. Aerodyn. 33, 171–180.
OpenFOAM, 2009. The Open Source CFD Toolbox, Programmer's Guide, Version 1.6. OpenCFD Limited.
Otsuki, Y., Fujii, K., Washizu, K., Ohya, A., 1978. Wind tunnel experiments on aerodynamic forces and pressure distributions of rectangular cylinders in a uniform flow. In: Proceedings of the Fifth Symposium on Wind Effects on Structures, pp. 169–176.
Rahman, M.M., Karim, M.M., Alim, M.A., 2007. Numerical investigation of unsteady flow past a circular cylinder using 2-D finite volume method. J. Naval Arch. Mar. Eng. 4, 27–42.
Sandham, N.D., Yao, Y.F., Lawal, A.A., 2003. Large-eddy simulation of transonic turbulent flow over a bump. Int. J. Heat Fluid Flow 24, 584–595.
Shimada, K., Ishihara, T., 2002. Application of a modified k–ε model to the prediction of aerodynamic characteristics of rectangular cross-section cylinders. J. Fluids Struct. 16, 465–485.
Shur, M., Spalart, P.R., Squires, K.D., Strelets, M., Travin, A., 2005. Three dimensionality in Reynolds-averaged Navier–Stokes solutions around two-dimensional geometries. AIAA J. 43, 1230–1242.
Sohankar, A., 2008. Large eddy simulation of flow past rectangular-section cylinders: side ratio effects. J. Wind Eng. Ind. Aerodyn. 96, 640–655.
Tamura, T., Ito, Y., 1996. Aerodynamic characteristics and flow structures around a rectangular cylinder with a section of various depth/breadth ratios. J. Struct. Const. Eng., Transfer Arch. Inst. Jpn. 486, 153–162.
Tian, X., Ong, M.C., Yang, J., Myrhaug, D., Chen, G., 2012. Three-dimensional effects of the flow normal to a flat plate at a high Reynolds number. In: Proceedings of the ASME 2012 31st International Conference on Ocean, Offshore and Arctic Engineering, ASME, Rio de Janeiro, Brazil.
Weller, H.G., Tabor, G., Jasak, H., Fureby, C., 1998. A tensorial approach to computational continuum mechanics using object-oriented techniques. Comput. Phys. 12, 620.
Wilcox, D.C., 1998. Turbulence Modeling for CFD, 2nd ed. DCW Ind., Inc., La Canada, CA.